nature chemistry

ARTICLES

https://doi.org/10.1038/s41557-018-0031-x

Cholesterol catalyses Aβ42 aggregation through a heterogeneous nucleation pathway in the presence of lipid membranes

Johnny Habchi[1,8], Sean Chia[1,8], Céline Galvagnion[1,7,8], Thomas C. T. Michaels[1,2], Mathias M. J. Bellaiche[1,3], Francesco Simone Ruggeri[1], Michele Sanguanini[1], Ilaria Idini[4], Janet R. Kumita[1], Emma Sparr[5], Sara Linse[4], Christopher M. Dobson[1], Tuomas P. J. Knowles[1,6] and Michele Vendruscolo[1*]

Alzheimer's disease is a neurodegenerative disorder associated with the aberrant aggregation of the amyloid-β peptide. Although increasing evidence implicates cholesterol in the pathogenesis of Alzheimer's disease, the detailed mechanistic link between this lipid molecule and the disease process remains to be fully established. To address this problem, we adopt a kinetics-based strategy that reveals a specific catalytic role of cholesterol in the aggregation of Aβ42 (the 42-residue form of the amyloid-β peptide). More specifically, we demonstrate that lipid membranes containing cholesterol promote Aβ42 aggregation by enhancing its primary nucleation rate by up to 20-fold through a heterogeneous nucleation pathway. We further show that this process occurs as a result of cooperativity in the interaction of multiple cholesterol molecules with Aβ42. These results identify a specific microscopic pathway by which cholesterol dramatically enhances the onset of Aβ42 aggregation, thereby helping rationalize the link between Alzheimer's disease and the impairment of cholesterol homeostasis.

Over 40 million people currently suffer from Alzheimer's disease worldwide, and as the global population ages, this number is predicted to approach 140 million by 2050[1]. The deposition of the amyloid-β peptide (Aβ) into insoluble aggregates in brain tissues is the molecular signature of the disease, with Aβ42, the 42-residue form of Aβ, being the major component of the deposits[2–5]. Understanding, at the molecular level, the effects of intrinsic and extrinsic factors on the aggregation process of Aβ42 is thus vital for developing effective therapeutic strategies aimed at inhibiting its self-assembly[6,7].

Among such factors, the disruption of lipid homeostasis in the brain is strongly associated with the pathogenesis of Alzheimer's disease[8,9]. Quite generally, lipids are found ubiquitously within the amyloid deposits formed by Aβ42[10], and it has also been suggested that comparative analysis of the lipid composition of the plasma and cerebrospinal fluid (CSF) of patients and healthy controls could lead to the identification of effective disease biomarkers and prognostic indicators of therapies for Alzheimer's disease[9,10].

A critical role of lipids in Alzheimer's disease is consistent with the fact that the ε4 allele of the apolipoprotein E gene (*APOE*) is the greatest currently known genetic risk factor for late-onset Alzheimer's disease[11,12]. Apolipoprotein E is a crucial regulator of cholesterol metabolism in the brain and of triglyceride metabolism throughout the body[13], and studies have shown that amyloid deposits fail to form in *APOE* knockout mice[14]. Therefore, much attention has been devoted to the link between Alzheimer's disease and cholesterol. Recent studies have suggested that plasma cholesterol levels are about 10% higher in Alzheimer's disease patients than in healthy individuals[15], and that cholesterol accumulates in senile plaques of patients and in mouse models of the disease[10,16]. Furthermore, it has also been suggested that statins, which are used to prevent cardiovascular diseases by lowering cholesterol levels, could also potentially reduce the risk of Alzheimer's disease[17]. Brain cholesterol, which exists primarily (>99.5%) in a non-esterified state, is largely formed in the myelin sheaths and cellular membranes of glial cells and neurons[18], represents about 25% of the total amount of cholesterol in the human body, and is important for neuronal development, synaptic plasticity and brain function. The impairment of cholesterol homeostasis could therefore be an important factor in the pathogenesis of the disease[19].

The mechanistic processes underlying the association of cholesterol with Alzheimer's disease remain, however, to be fully established[20,21]. Evidence for a possible causative role is provided by recent studies showing that modulating cholesterol levels can regulate Aβ aggregation[20]. For example, depleting cholesterol in hippocampal neurons in animal models of Alzheimer's disease has been found to reduce Aβ42 aggregate levels, while raising it leads to their increase[24]. Additionally, lipid rafts, which are domains in cellular membranes enriched in cholesterol and sphingolipids, have been implicated in the processing of the amyloid precursor protein (APP) through which Aβ is generated[9,10,25]. Moreover, the region of residues 22–35 in the Aβ sequence has been identified as a potential binding site of cholesterol[21].

Although an interaction between Aβ42 and cholesterol has already been reported[26], the specific mechanisms by which it occurs and affects Aβ42 aggregation have not yet been fully identified.

[1]Centre for Misfolding Diseases, Department of Chemistry, University of Cambridge, Cambridge, UK. [2]Paulson School for Engineering and Applied Sciences, Harvard University, Cambridge, USA. [3]Laboratory of Chemical Physics, National Institute of Diabetes and Digestive and Kidney Diseases, National Institutes of Health, Bethesda, MD, USA. [4]Department of Biochemistry & Structural Biology, Center for Molecular Protein Science, Lund University, Lund, Sweden. [5]Division of Physical Chemistry, Department of Chemistry, Lund University, Lund, Sweden. [6]Department of Physics, Cavendish Laboratory, Cambridge, UK. [7]Present address: German Center for Neurodegenerative Diseases (DZNE), Bonn, Germany. [8]These authors contributed equally: Johnny Habchi, Sean Chia, Céline Galvagnion. *e-mail: mv245@cam.ac.uk

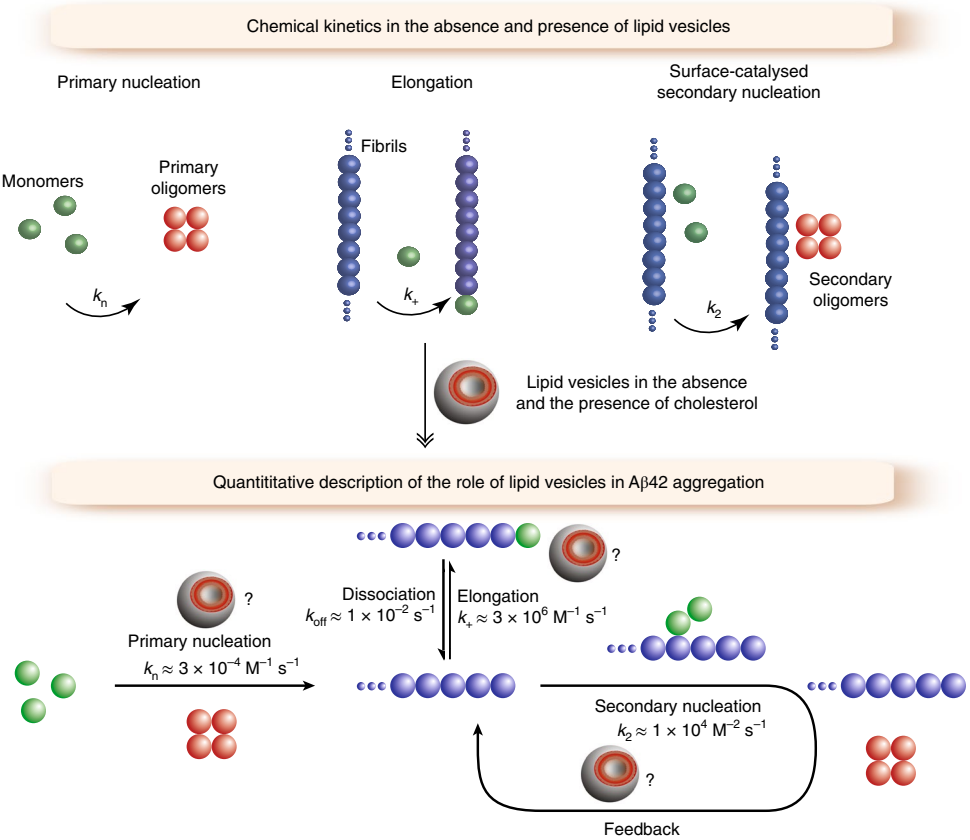

Fig. 1 | Schematic illustration of the strategy used in the present work. Aβ42 aggregation kinetics were performed in the absence and presence of DMPC lipid vesicles that were either free of cholesterol, or contained different concentrations of cholesterol. Subsequently, the effects of the lipid vesicles were assessed on the individual microscopic steps of Aβ42 aggregation.

For instance, the reduction in the rate of Aβ42 aggregation observed in the presence of 1,2-dipalmitoyl-*sn*-glycero-3-phosphocholine (DPPC) gel phase membranes was abolished on adding cholesterol to form liquid ordered bilayer membranes[27]. By contrast, other studies have suggested that cholesterol can inhibit interactions between Aβ and lipid membranes, thus increasing the extracellular levels of Aβ and promoting its aggregation[28].

To investigate this problem, we analysed quantitatively the direct effects of cholesterol on Aβ42 aggregation using the strategy illustrated in Fig. 1. Our approach exploits the recent development of highly reproducible thioflavin-T (ThT)-based kinetic measurements and analytical approaches to their interpretation[29,30]. Such measurements have made it possible to show that the aggregation of Aβ42 is characterized by a surface-catalysed secondary nucleation process, where the fibril surfaces act as catalytic sites for the generation of toxic Aβ42 oligomers. The generated oligomers can grow further and convert into fibrils, promoting the formation of additional toxic species in a highly effective catalytic cycle[22,30–35].

Analysis of the reaction kinetics has also been powerful in characterizing the effects of intrinsic and extrinsic factors on the rates of individual microscopic steps in the aggregation process of Aβ42[23,36,37]. In particular, the diverse pathways through which macromolecules, such as molecular chaperones and antibodies, can affect the aggregation of Aβ42 have recently been described in detail[23,36,37,38]. Moreover, using the same approach, the effects of disease-associated mutations and pH variations could be deciphered, showing that both factors can give rise to enhancements in the secondary nucleation process[34]. It has also been shown that the effects of small molecules on the different microscopic steps of the Aβ42 aggregation process can also be monitored in detail, thus leading to the development of a chemical kinetics-based drug discovery strategy that aims at identifying drug candidates that can inhibit specific steps in the aggregation reaction of Aβ42[39,40].

In the present study, we extended this kinetics-based strategy to decipher the role of cholesterol in modulating Aβ42 aggregation. To this end, we characterize at the molecular level the effects of vesicles prepared with 1,2-dimyristoyl-*sn*-glycero-3-phosphocholine (DMPC) and cholesterol (DMPC:cholesterol vesicles) on the microscopic steps of Aβ42 aggregation (Fig. 1). Our results indicate that these vesicles provide a model membrane that can effectively increase the nucleation rate of Aβ42. Furthermore, we show that, despite the occurrence of a cholesterol-dependent nucleation process, surface-catalysed secondary nucleation remains the dominant mechanism for aggregate proliferation, as in the lipid-free aggregation process. We then provide evidence that primary oligomers of Aβ42, whether they are formed through homogeneous or heterogeneous nucleation events, are likely to possess structural similarities by showing that a previously characterized inhibitor of the homogeneous nucleation of Aβ42 aggregation also inhibits the heterogeneous primary nucleation events catalysed by lipid vesicles[39].

Overall, these results reveal a self-assembly process that includes a heterogeneous primary nucleation step through which Aβ42 aggregates in the presence of DMPC:cholesterol vesicles. This step can be significantly faster than that of homogeneous primary nucleation, leading to the more rapid formation of potentially neurotoxic oligomers. We therefore propose a mechanism to explain how the presence of cholesterol can accelerate Aβ42 aggregation, thus enhancing our understanding of the molecular origins of Alzheimer's disease and potentially contributing to the development of effective therapeutics against this devastating condition.

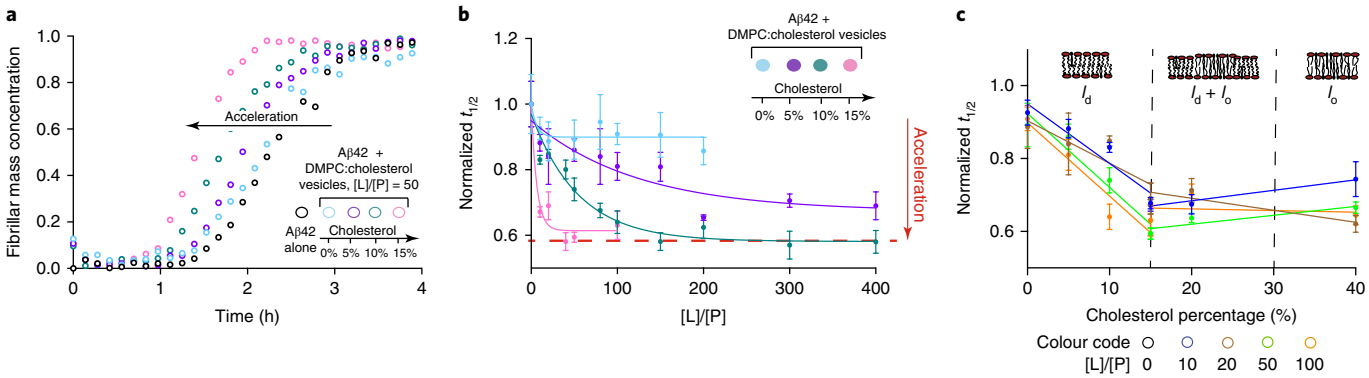

Fig. 2 | DMPC:cholesterol vesicles accelerate Aβ42 aggregation. a, Comparison of kinetic profiles for the aggregation of a 2 μM Aβ42 sample in the presence of either DMPC vesicles or of DMPC:cholesterol vesicles containing increasing concentrations of cholesterol up to 15% at a lipid-to-protein ([L]/[P]) ratio of 50. **b**, Evolution of normalized $t_{1/2}$ values of the aggregation kinetics of Aβ42 against [L]/[P] as derived from the data in Supplementary Fig. 1. **c**, Evolution of normalized $t_{1/2}$ values of the aggregation kinetics of Aβ42 against the percentage of cholesterol within the membrane as derived from the data in Supplementary Figs. 1–3. Note the change of the DMPC membrane properties from a single liquid disordered phase (l_d) to a liquid ordered phase (l_o) in the presence of increasing concentrations of cholesterol. Throughout, error bars indicate standard deviation among independent replicates.

Results

Cholesterol-containing lipid vesicles accelerate Aβ42 aggregation. To decipher the role of cholesterol in Aβ42 aggregation, we carried out a global kinetic analysis of its effect on the Aβ42 aggregation process[29] in the presence of zwitterionic vesicles containing cholesterol at concentrations ranging from 0 to 40 mol% of the total lipid concentration (Fig. 2 and Supplementary Figs. 1–4). We investigated this range because cholesterol accounts for about 20% of the total content of brain lipids, although its levels in neuronal membranes can vary substantially from one cell or organelle to another[41,42]. Thus, for example, the outer monolayer of plasma membranes has cholesterol levels of around 30 mol%, while these levels are much lower in the corresponding inner monolayer[43].

Because phosphatidylcholine (PC) lipids, together with phosphatidylethanolamine (PE) and phosphatidylserine (PS) lipids, constitute the most abundant components of neuronal membranes[44], we investigated the effects of cholesterol on Aβ42 aggregation for a series of model systems composed of zwitterionic PC lipids with different acyl-chain compositions in terms of the length and degree of unsaturation (DMPC (two chains C14:0), POPC (C18:1 and C16:0) and DOPC (two chains C18:1)). We found that the level of unsaturation alters, to different extents, the effects of cholesterol on Aβ42 aggregation, with the rate of aggregation increasing with the degree of unsaturation of the PC hydrocarbon chain (DOPC > POPC > DMPC) (Supplementary Figs. 1 and 4). These findings may be explained by the increased exposure to the hydrophobic hydrocarbon segment of the bilayer for the unsaturated lipids with bulky hydrocarbon chains, as the average accessible area per PC headgroup in the bilayer varies from 60 Å^2 for DMPC to 69 Å^2 for 1-palmitoyl-2-oleoyl-*sn*-glycero-3-phosphocholine (POPC) and 72 Å^2 for 1,2-dioleoyl-*sn*-glycero-3-phosphocholine (DOPC)[45,46]. By contrast, although anionic lipids, such as PS, can significantly influence Aβ42 aggregation and the structures of the aggregates[47,48], they are mainly found in the inner leaflet of the plasma membrane, and therefore are not enriched in the regions where cholesterol is primarily located.

Therefore, to assess specifically and systematically the effects of cholesterol on the aggregation of Aβ42 in a physiologically relevant system, we used model systems composed of DMPC and cholesterol, which capture several important features of the behaviour of cholesterol in membranes that are highly relevant to lipid rafts[49], including the formation of small-scale domains and of the liquid ordered membrane structure[50–52]. The advantage of these model systems is that DMPC alone does not significantly influence Aβ42 aggregation (Supplementary Fig. 1), making it possible to identify clearly the effects of the added cholesterol.

Using DMPC:cholesterol vesicles, we found that increasing cholesterol content significantly enhanced Aβ42 aggregation (Fig. 2 and Supplementary Figs. 1–3). These results also show that the effects of the lipid vesicles on the aggregation behaviour depend on both the lipid-to-protein (L/P) ratio (mol:mol) (Fig. 2b) and the cholesterol content within the membrane (Fig. 2c). We also observed similar behaviour when we added cholesterol to model membranes composed of DMPC and 1,2-dimyristoyl-*sn*-glycero-3-phosphoethanolamine (DMPE), further supporting the conclusion that the presence of cholesterol promotes Aβ42 aggregation (Supplementary Fig. 5)[53,54]. Moreover, we observed a broadening of the DMPC melting transition and an increase in the size and fluidity of the DMPC vesicles with increasing concentrations of cholesterol (Supplementary Figs. 6 and 7)[55,56]. In addition, we found that the acceleration of the aggregation kinetics of Aβ42 was not directly related to an increase in the size of the vesicles (Supplementary Fig. 8).

A maximum effect corresponding to a decrease by about 35–40% in the half-time of the aggregation reaction was observed at [L]/[P] ratios above 200 for vesicles containing 5% and 10% cholesterol (Fig. 2b). For all [L]/[P] ratios, the acceleration in the aggregation kinetics of Aβ42 shows a strong dependence on the membrane composition up to a cholesterol content of about 15 mol%, and the acceleration appears to be unaffected by further increases in cholesterol (Fig. 2 and Supplementary Figs. 1–3). This nonlinear response of the aggregation kinetics to the concentration of cholesterol suggests that specific changes in the membrane properties are crucial to the aggregation process[57,58]. These results can be rationalized by observing that in a PC lipid system at 37 °C, a single liquid disordered (l_d) phase is present at cholesterol contents below 15%. In such a situation, the cholesterol molecules are homogeneously solubilized in the bilayer, gradually changing its properties and composition with increasing cholesterol content (Fig. 2c). When the cholesterol content exceeds 15 mol%, the system segregates into small-scale domains ('rafts') composed of l_d and liquid ordered (l_o) phases. At cholesterol contents above 30 mol%, however, a single l_o phase is formed, and over the whole range of domain formation, the compositions in the segregated l_d and l_o domains are unchanged and determined by the compositions at the phase boundaries, with the proportions of the different domains varying with cholesterol content.

To exclude possible interference of the lipid vesicles with the ThT fluorescence signal, Aβ42 aggregation was also monitored by

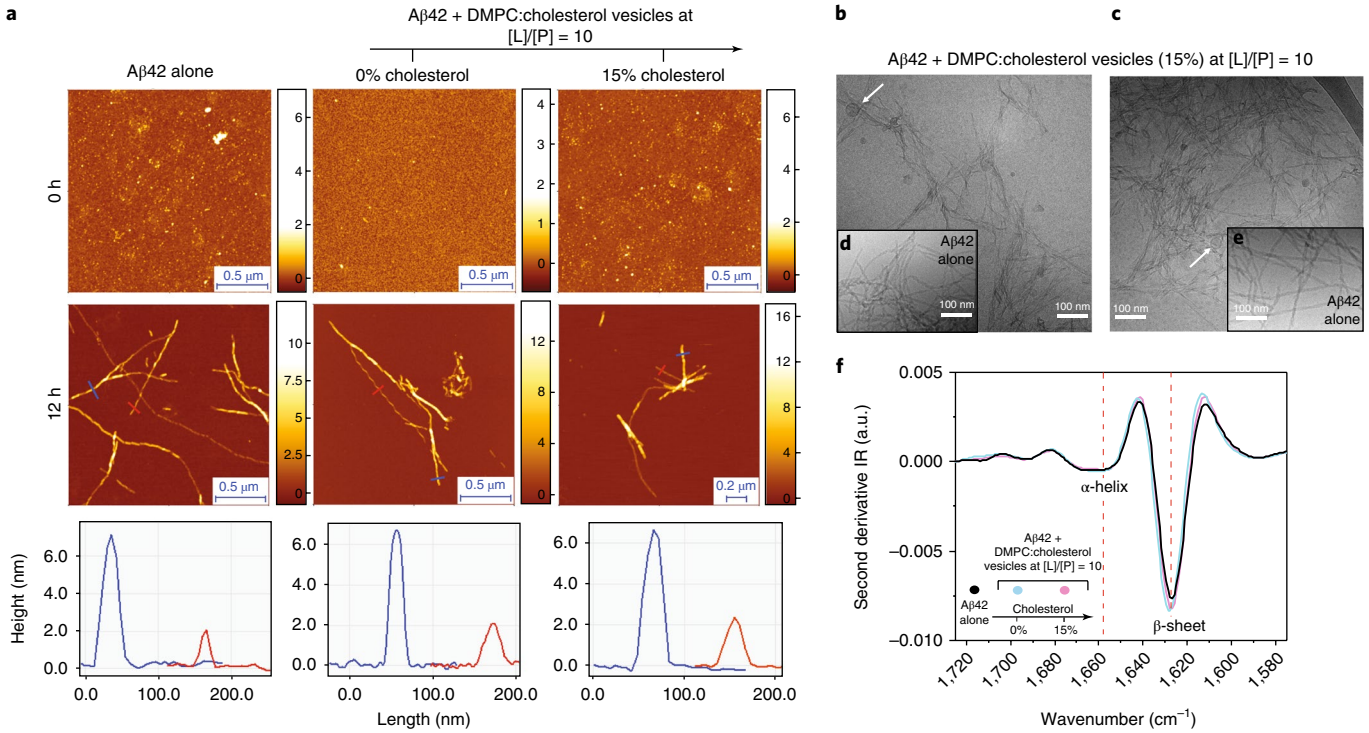

Fig. 3 | Biophysical characterization of the effects of DMPC:cholesterol vesicles on Aβ42 fibrils. a, AFM morphology maps of ThT-free Aβ42 samples at time 0 h and after 12 h incubation at 37 °C in the absence or presence of DMPC:cholesterol vesicles containing 0% or 15% cholesterol at a [L]/[P] ratio of 10. Similar height distributions are observed for Aβ42 fibrils irrespective of whether they are formed in the absence or the presence of lipid vesicles (red and blue marks on the images). **b**–**e**, Cryo-EM images of ThT-free Aβ42 fibrils: two representative images of Aβ42 fibrils formed in the presence of DMPC:cholesterol vesicles containing 15% cholesterol at a [L]/[P] ratio of 10 (**b**,**c**) and two representative images formed in their absence (**d**,**e**). White arrows indicate the presence of the vesicles. **f**, Second derivative of the IR amplitude of Aβ42 fibrils formed in the absence or presence of DMPC:cholesterol vesicles containing 0% or 15% cholesterol at a [L]/[P] ratio of 10.

circular dichroism (CD) spectroscopy (Supplementary Fig. 9)[59]. We recorded time-dependent CD spectra of a 20 μM Aβ42 solution in the absence or presence of DMPC vesicles with either 0% or 15% cholesterol at a [L]/[P] ratio of 10 (Supplementary Fig. 9). At time 0, the CD spectrum of Aβ42 exhibited a negative mean residue ellipticity (MRE) at about 200 nm, which is characteristic of a disordered peptide. At the end of the reaction, however, the spectrum included positive and negative MRE values at about 200 nm and 218 nm, characteristic of the presence of β-sheet structure. The time dependence of the MRE values at 218 nm (MRE_{218nm}) in the presence of vesicles at a [L]/[P] ratio of 10 shows that β-sheet formation occurs at a slightly slower rate in the presence of DMPC vesicles than in their absence (Supplementary Fig. 9). This difference could arise from the multiple general contributions of foreign surfaces provided by both the cuvette and the lipid, as of which could affect the aggregation process[60]. By comparing the spectra over time in the presence of DMPC:cholesterol vesicles containing 15% cholesterol, and in the presence of vesicles free of cholesterol, where general additional contributions from surface effects are similar, we observed that the formation of β-sheet structure of Aβ42 occurs more rapidly in the presence of DMPC:cholesterol vesicles than in DMPC vesicles free of cholesterol, in agreement with the results obtained using ThT-based kinetics (Supplementary Fig. 9).

Morphology and structure of Aβ42 fibrils in the presence of cholesterol-containing lipid vesicles. Using atomic force microscopy (AFM) we acquired high-resolution 3D morphology maps of Aβ42 fibrils formed in the absence and presence of DMPC vesicles, the latter both free of cholesterol or containing 15% cholesterol at a [L]/[P] ratio of 10 (Fig. 3a)[61]. No significant differences in the length and height of the fibrils could be observed between the samples. Also, by using cryo-electron microscopy (cryo-EM), we found that fibrils formed in the presence of vesicles with 15% cholesterol (Fig. 3b,c) are of similar length and thickness as those formed by Aβ42 alone (Fig. 3d,e). However, the fibrils appeared to be organized slightly differently, implying that they could have altered surface properties. Previous observations of the presence of lipids in amyloid plaques[10] suggest that lipids may be incorporated in the aggregates; indeed, few vesicles are seen, suggesting that such incorporation may have occurred (Fig. 3b,c). To investigate further the structural organization of the fibrillar aggregates, we used Fourier-transform infrared (FTIR) spectroscopy (Fig. 3f and Supplementary Fig. 10). The IR absorption of proteins is characterized by a series of amide bands, with the shape and position of the amide band I providing information on their secondary and quaternary structures[62]. We found identical amide I bands, and thus similar structural organization of the ThT-free Aβ42 fibrils within experimental error, as also demonstrated by the comparison of their second derivatives (Fig. 3f and Supplementary Fig. 10). In addition, we carried out fluorescence measurements that show that the spectra of ThT bound to Aβ42 fibrils are similar in the presence and absence of the cholesterol-containing lipid vesicles during fibril formation (Supplementary Fig. 10).

DMPC:cholesterol vesicles accelerate the rate of Aβ42 primary nucleation by up to 20-fold. We carried out a quantitative analysis of Aβ42 aggregation in the presence of lipid vesicles to define the changes in the rate constants governing each microscopic step. The analysis of t_{lag} (the time required for the ThT fluorescence intensity to reach 10% of its final value) and t_{growth} (the time required for

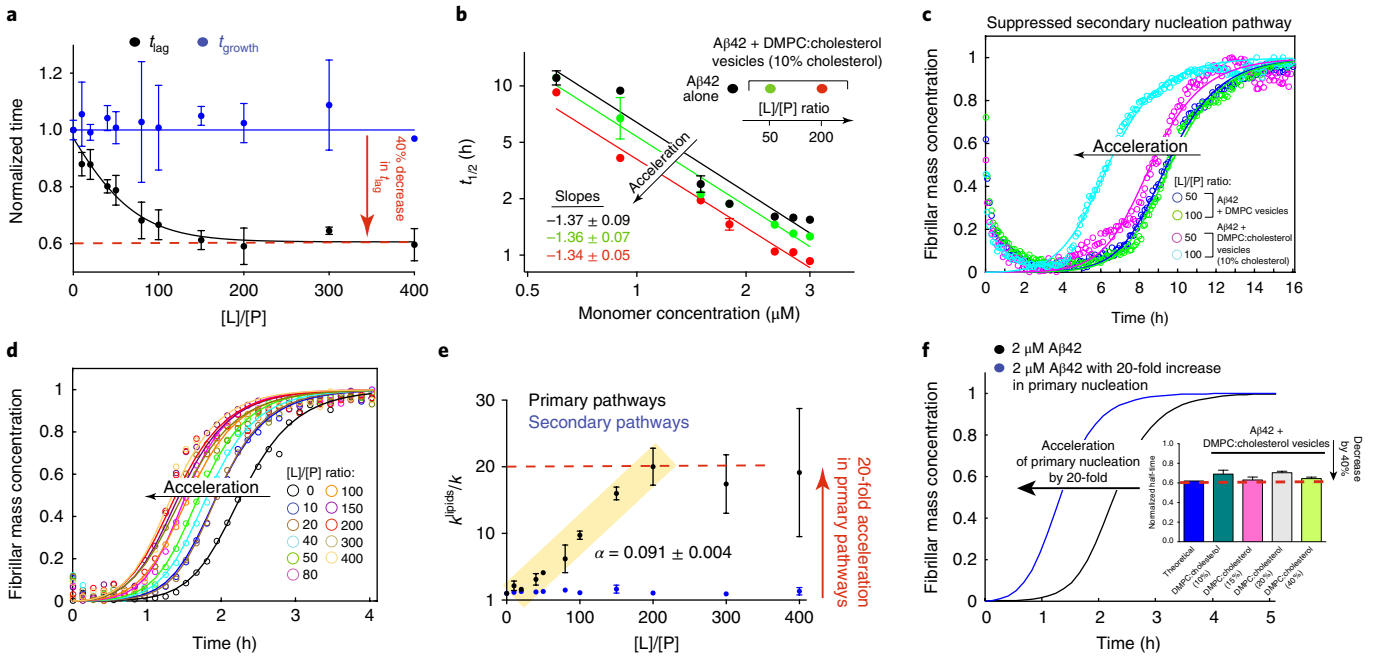

Fig. 4 | DMPC:cholesterol vesicles accelerate Aβ42 primary nucleation by up to 20-fold through a heterogeneous nucleation process. a, Comparison of the normalized t_{lag} and t_{growth} values derived from the aggregation profiles of 2 μM Aβ42 in the presence of increasing concentrations of DMPC:cholesterol vesicles containing 10% cholesterol as a function of [L]/[P] ratio (Supplementary Fig. 1). **b**, The half-time, $t_{1/2}$, of Aβ42 aggregation as a function of the initial Aβ42 monomer concentration in the absence or presence of DMPC:cholesterol vesicles containing 10% cholesterol at [L]/[P] ratios of 50 and 200. **c**, Kinetic profiles of the aggregation reaction of 1.2 μM Aβ42 in the presence of one molar equivalent of Brichos (1.2 μM), and DMPC or DMPC:cholesterol vesicles containing 10% cholesterol at [L]/[P] ratios of 50 and 100. Solid lines show predictions for the resulting reaction profiles when the rate constants of the primary pathways are modified to include the lipid-induced nucleation process. **d**, Aggregation profiles of 2 μM Aβ42 in the absence and presence of DMPC:cholesterol vesicles containing 10% cholesterol at increasing [L]/[P] ratios. Solid lines show predictions for the resulting reaction profiles when the rate constants of the primary and secondary pathways are modified to include the lipid-induced nucleation process. **e**, Evolution of apparent reaction rate constants with increasing [L]/[P] ratios of DMPC:cholesterol vesicles containing 10% cholesterol. k^{lipids}/k represents in each case either $k_+'k_n'/k_+k_n$ or $k_+'k_2'/k_+k_2$, where k_n', k_+' and k_2' are the apparent rate constants of primary nucleation, elongation and secondary nucleation, respectively, in the presence of vesicles. Note the significant increase in $k_+'k_n'$ as compared to $k_+'k_2'$ as [L]/[P] increases (in the yellow zone). **f**, Numerical calculations of the reaction profiles for a solution of 2 μM Aβ42 with (blue) and without (black) an increase by 20-fold of the rate constant of primary nucleation, k_n' (see Methods). Inset, $t_{1/2}$ values of the calculated and experimental curves showing a maximal effect of lipids. Throughout, error bars indicate standard deviation among independent replicates.

the ThT fluorescence intensity to reach 90% of its final value after t_{lag}) of Aβ42 aggregation shows that these vesicles have a concentration-dependent effect on t_{lag} but no significant effect on t_{growth} (Fig. 4a). These results indicate that the primary nucleation pathway is the main microscopic process perturbed by the presence of DMPC:cholesterol vesicles[23,63]. In addition, the scaling exponent of the Aβ42 concentration dependence, which reflects the dominance of the fibril-catalysed secondary nucleation process[31], remained unaffected within error limits, with a value close to −1.3 in the presence of the cholesterol-containing vesicles (Fig. 4b).

We then carried out an additional series of measurements of the aggregation kinetics of Aβ42 under conditions where the surface-catalysed secondary nucleation was suppressed by a molecular chaperone, the Brichos domain[37] (Fig. 4c and Supplementary Fig. 11). In the presence of Brichos, Aβ42 aggregation is mainly driven by primary nucleation and elongation because surface-catalysed secondary nucleation is suppressed (Supplementary Fig. 11). We found that the aggregation kinetics of Aβ42 were significantly accelerated in the presence of DMPC:cholesterol vesicles, and to a much smaller extent when the vesicles are free of cholesterol (Fig. 4c). Thus, the observed effects can be attributed to an increase in the rates of primary nucleation and/or elongation when cholesterol is incorporated into DMPC vesicles.

Next, to define more quantitatively how cholesterol affects the microscopic rates, we modified the underlying kinetic equations (equations (1) and (2)) to account for the addition of a lipid-induced aggregation process to the three microscopic events (primary nucleation, surface-catalysed secondary nucleation and elongation) involved in the aggregation pathway of Aβ42. We analysed the aggregation profiles using these modified equations, which relate the macroscopic time evolution of the fibril mass to the rate constants of the different microscopic events. We found the best fits when the rates of the primary pathway (k_+k_n) were significantly increased, and the secondary pathways (k_+k_2) were relatively unaffected (Fig. 4d,e). These results indicate that DMPC:cholesterol vesicles are mainly involved in enhancing the primary nucleation process, rather than the elongation process. Similar results were obtained for DMPC:cholesterol vesicles containing cholesterol levels as low as 5% (Supplementary Fig. 12). Additionally, the best fits of the Aβ42 aggregation kinetics in the presence of Brichos and DMPC:cholesterol vesicles correspond to an increase only in the rate of primary nucleation, thus further confirming the role of DMPC:cholesterol vesicles in accelerating the primary processes in Aβ42 aggregation (Supplementary Fig. 11).

Taken together, these data indicate that the DMPC:cholesterol vesicles act as catalysts of Aβ42 aggregation by increasing the formation of primary oligomers, thereby accelerating the overall aggregation kinetics. Thus, cholesterol introduces heterogeneous primary nucleation as an additive active process into the Aβ42 aggregation pathway. Thus, the primary nucleation of Aβ42 occurs through two

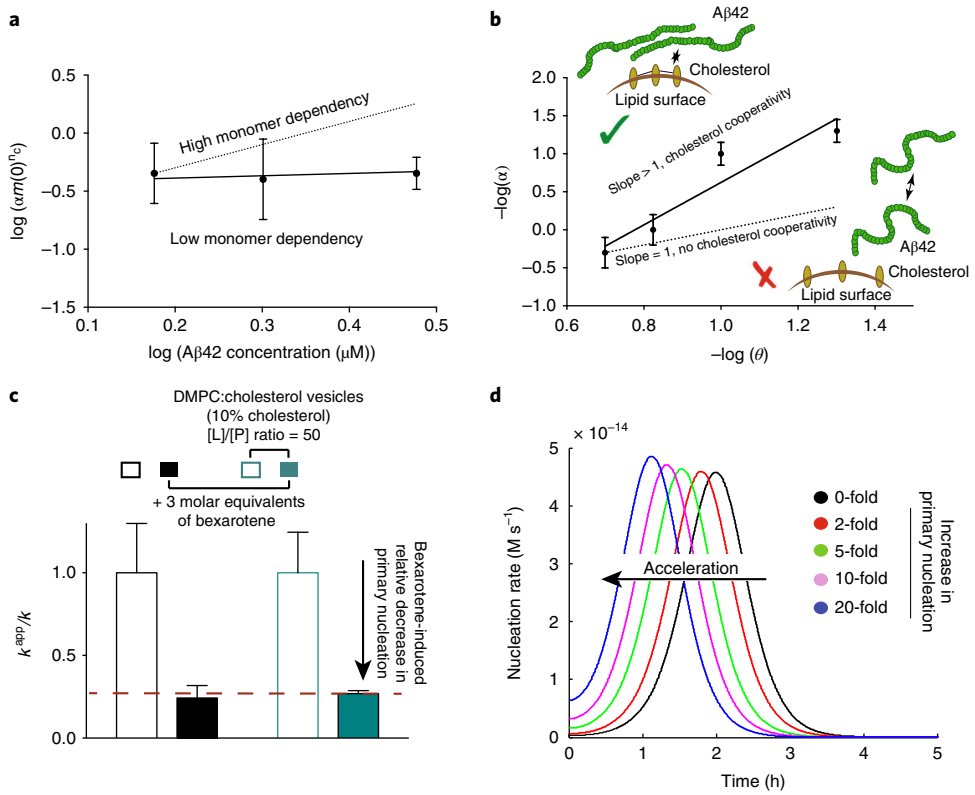

Fig. 5 | DMPC:cholesterol vesicles catalyse the formation of Aβ42 oligomers through heterogeneous nucleation. a, Log–log plot of $\alpha m(0)^{n_c}$ as a function of the initial concentration of Aβ42 monomers, $m(0)$. **b**, Log–log plot of α, the slope of the acceleration ε of primary nucleation, as a function of θ, the surface coverage by cholesterol (% of cholesterol within the membrane). A schematic representation of the Aβ42 heterogeneous primary nucleation process on DMPC:cholesterol vesicles is also shown. Note that heterogeneous primary nucleation occurs as a result of the cooperativity in the interaction of several cholesterol molecules with Aβ42. **c**, Ratio of the apparent primary nucleation rate constants in the absence (black) and presence (green) of DMPC:cholesterol vesicles containing 10% cholesterol at a [L]/[P] ratio of 50, either in the presence or absence of 3 molar equivalents of bexarotene to Aβ42. k_n is the rate constant of homogeneous primary nucleation and k_n' is the sum of the rate constants of both homogeneous and heterogeneous primary nucleation, k^{app}/k represents either $k_n'^{app}/k_n$ (the decrease in the apparent primary nucleation rate constant when bexarotene is added to Aβ42 in the presence of DMPC:cholesterol vesicles) or k_n^{app}/k_n(the decrease in the apparent primary nucleation rate constant when bexarotene is added to Aβ 42 in the absence of DMPC:cholesterol vesicles). **d**, Acceleration in the formation of the total number of oligomers generated through increasing rates of primary nucleation. Error bars in **a** and **b** were derived from the extrapolation of data from Supplementary Figs. 13 and 1–3, respectively. Error bars in **c** indicate standard deviation between independent replicates.

distinct mechanisms, a homogeneous pathway (with rate constant k_n) where new aggregates are formed solely from the interactions between soluble monomers, and a heterogeneous pathway where new aggregates are generated at a rate k_{cat} that depends on the concentrations of both monomeric Aβ42 and lipid vesicles. Hence, the overall rate constant of Aβ42 primary nucleation becomes k_n', which accounts for the contribution of both k_n and k_{cat} to the initial step of aggregation (see Methods).

Heterogeneous primary nucleation depends on the concentration of Aβ42 monomers and on the number of accessible sites for each peptide, s (in [L]/[P]), of the DMPC:cholesterol vesicles. Indeed, a steep linear increase with the [L]/[P] ratio in the primary pathways was observed for DMPC:cholesterol vesicles containing 10% cholesterol at [L]/[P] ratios below 200 (Fig. 4e). In the case of DMPC:cholesterol vesicles containing 5% cholesterol, saturation could not be observed even in the presence of [L]/[P] ratios as high as 400 (Supplementary Fig. 12). In all cases, the heterogeneous primary nucleation was found to be linearly dependent on the [L]/[P] ratio, and consequently on the number of accessible sites for each peptide s, before saturation is reached (see Methods). At high concentrations of accessible sites, that is, at [L]/[P] ratios above 200 in the case of DMPC:cholesterol vesicles containing 10% cholesterol, where the heterogeneous primary nucleation is likely to be restricted by the adsorption and desorption rates of the peptide, the relative increase in the heterogeneous primary nucleation rate is maximal and corresponds to an increase by a factor of 20 ± 2 relative to the homogeneous primary nucleation rate in the absence of cholesterol-containing vesicles (Fig. 4e). We next carried out a numerical estimate of the rate of formation of the total mass of Aβ42 aggregates in which we increased the rate of primary nucleation by 20-fold (Fig. 4f). In agreement with the results of all the experiments performed in the presence of cholesterol to achieve a maximum rate of Aβ42 aggregation (Fig. 4f, inset), we found that the theoretical $t_{1/2}$ is smaller than that of Aβ42 alone by about 40% (Figs. 2b and 4f). A theoretical prediction based on the analytical solution for the aggregation kinetics[64–66] indicates that an increase in the rate of primary nucleation of an aggregation reaction translates into a decrease of about 34% in the reaction $t_{1/2}$, which is fully consistent with the experiments reported here (see Methods).

Chemical kinetics characterize the roles of Aβ42 monomers and cholesterol in DMPC:cholesterol vesicles in the heterogeneous primary nucleation step. The relative acceleration, ε, of the effective rate of primary nucleation in Aβ42 aggregation due

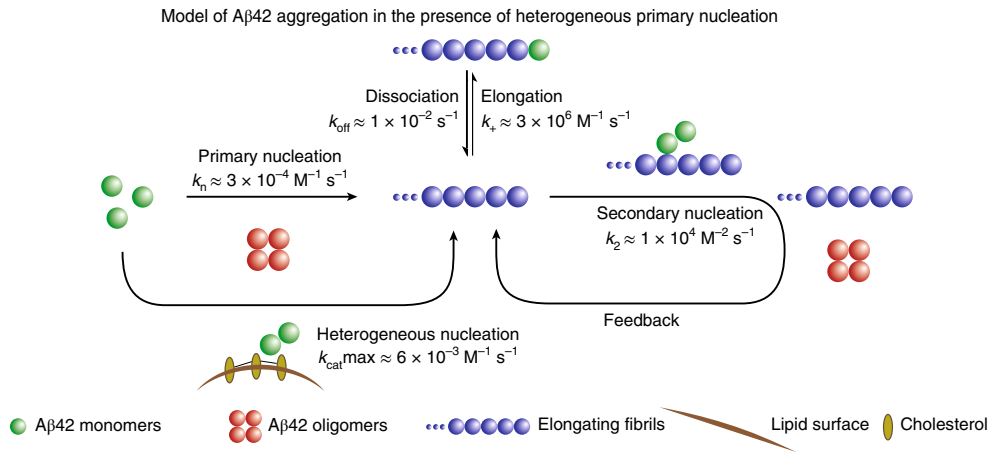

Fig. 6 | DMPC:cholesterol vesicles introduce a heterogeneous nucleation pathway in the Aβ42 aggregation process. Scheme showing the proposed model of Aβ42 aggregation in the presence of catalytic sites formed by DMPC:cholesterol membranes. In the presence of DMPC:cholesterol vesicles, the primary nucleation of Aβ42 occurs through either homogeneous nucleation, in which Aβ42 nuclei are formed solely from the interactions of Aβ42 monomers, or through heterogeneous nucleation, in which Aβ42 nuclei are formed from the interactions of Aβ42 monomers and lipid membranes. In either type of primary nucleation, once a critical number of fibrils is formed, secondary nucleation becomes the major source for generating new oligomers.

to the introduction of a lipid-associated heterogeneous pathway is dependent on the concentration of Aβ42 monomers, $m(0)$, as well as the accessibility factor, σ, of the lipid system, which we found to be dependent on the proportion of cholesterol within the lipid membrane (equation (9)). We thus set out to characterize in detail the contributions to the heterogeneous primary nucleation pathway of the various species involved, including the Aβ42 monomers and the fraction of cholesterol in DMPC:cholesterol vesicles.

First, we observed that the total lipid concentration of the DMPC:cholesterol vesicles containing 10% cholesterol required for a maximum rate of Aβ42 aggregation was higher at increasing concentrations of Aβ42 (Supplementary Fig. 13). This observation implies that ε decreases as the concentration of Aβ42 monomers decreases. Considering that α (equation (10)) describes the relative increase in the primary nucleation rate due to the additional heterogeneous primary nucleation per accessible site for each peptide, a double logarithmic plot of $\alpha m(0)^{n_c}$ against the initial monomer concentration, $m(0)$, yields a line with slope n_h, which corresponds to the monomer concentration dependency of the heterogeneous nucleation pathway (Fig. 5a and Methods). The low reaction order observed for n_h ($n_h < 2$) suggests that, over the range of monomer concentrations probed in our experiments (1.5–3 μM), the coverage of a single nucleation site by monomers could be saturated, such that the heterogeneous nucleation pathway in this case is primarily dependent on the number of accessible sites for each peptide [L]/[P] (see section Methods).

As observed above, the maximum rate of Aβ42 aggregation occurred at different [L]/[P] ratios for different cholesterol contents of DMPC:cholesterol vesicles (Fig. 2b,c and Supplementary Figs. 1–3). These effects were found to depend, in a nonlinear manner, on cholesterol concentration, suggesting that the organisation of cholesterol within the DMPC:cholesterol membranes may be responsible for creating the number of accessible sites for each peptide, s, for Aβ42 nucleation. To explain these findings, we hypothesized that the relative increase in the rate of primary nucleation, α, might be controlled by the presence of multiple cholesterol molecules. From the probability of observing m adjacent sites occupied by cholesterol molecules, $p = \theta^m$, where θ denotes the surface coverage by cholesterol, that is, the percentage of cholesterol within the membrane, we found the accessibility factor $\sigma \sim \theta^m$. To test this prediction, we plotted α as a function of θ in a log–log plot, finding a line with slope $m > 1$ (Fig. 5b). This result indicates that the number of accessible sites for each peptide is correlated with the higher-order assembly of cholesterol molecules within the DMPC:cholesterol membrane. Therefore, under these conditions, at the maximal acceleration of Aβ42 aggregation, where the primary pathways are accelerated 20-fold, assuming that the catalysis involves several molecules of cholesterol, the total number of catalytic sites is approximately 10% the number of Aβ42 monomers (see Methods). These results imply the presence of positive cooperativity in the interaction of Aβ42 with cholesterol-containing membranes, and that a further increase in the number of catalytic sites does not increase the aggregation rate. The total number of primary nucleation sites estimated in this way is found to be at least two orders of magnitude higher than the number of primary nucleation sites required for a maximal effect to occur.

We then explored whether or not Aβ42 oligomers formed as a result of heterogeneous primary nucleation possess similar structural features to those formed by homogeneous primary nucleation. Because primary nuclei are formed transiently during the aggregation process, their direct structural characterisation is very challenging[6]. We therefore investigated their structural properties using bexarotene, a small molecule that inhibits Aβ42 primary nucleation, as a probe (Fig. 5c and Supplementary Fig. 14)[39]. We found that bexarotene inhibits Aβ42 primary nucleation irrespective of whether the primary oligomers of Aβ42 are formed through homogeneous or heterogeneous nucleation. These results suggest that the nuclei generated through homogeneous or heterogeneous primary nucleation share common structural features (Fig. 5c and Supplementary Fig. 14).

We then estimated the total rate of formation of oligomers from both primary and secondary processes in the aggregation of a 2 μM solution of Aβ42 in the absence and presence of DMPC:cholesterol vesicles containing increasing concentrations of cholesterol (see Methods). We found that increasing the rate of primary nucleation increases the reaction rate of the aggregation without affecting significantly the total load of toxic oligomers generated during the reaction[23,31,36,37,39,40]. Consistently, our calculations show that increasing the rate of Aβ42 primary nucleation in the presence of DMPC:cholesterol vesicles is accompanied by earlier formation of oligomers (Fig. 5d).

Discussion

It is increasingly recognized that changes in lipid homeostasis can influence the levels of toxic species formed by Aβ42, as indicated

Table 1 | Estimation of the numbers of accessible primary nucleation sites, r_{sites}, per Aβ42 monomer for given monomer to lipid concentration ratios

θ	[L]/[P] at maximal effect	r_{sites}
0.05	400	0.05
0.10	200	0.20
0.15	20	0.07
0.20	10	0.08

θ is the surface coverage by cholesterol.

by the results of recent experiments carried out both in cell cultures and in rabbit models[24,67]. Moreover, the kinetics of Aβ42 oligomerisation and amyloid formation in vitro have been found to be affected by the presence of specific lipids including gangliosides and sphingomyelin[68].

To help rationalize these findings, we have identified here a mechanism by which a specific lipid involved in the pathology of Alzheimer's disease influences the process of Aβ42 aggregation. We have shown, therefore, that cholesterol-containing vesicles provide an alternative heterogeneous primary nucleation route that results in a faster rate of formation of oligomeric species.

These results provide insights into the potential pathological role of Aβ42 in brain tissue. For typical cellular volumes (0.3–5 pl) and physiological levels of Aβ42 (1–10 nM), based on equation (6), we can estimate that it would take on average between 10 and 300 years for the Aβ42 aggregation process to occur spontaneously. We found, however, that the onset of Aβ42 aggregation is accelerated up to 20 times by the heterogeneous primary nucleation pathway created by DMPC:cholesterol vesicles, thus dramatically reducing the average nucleation times to the range of months to decades. Although these estimates are only indicative, as they do not reflect the complexity of the cellular environment, they illustrate how heterogeneous nucleation processes can substantially accelerate the formation of Aβ42 species (Fig. 6).

Overall, our results indicate that while spontaneous Aβ42 aggregation may be a rather slow process, triggering it through heterogeneous nucleation pathways can increase substantially the rate of aggregation, suggesting that cholesterol, or other compounds with a similar effect on Aβ42 aggregation, could indirectly constitute a risk factor for Alzheimer's disease.

By describing a molecular mechanism through which DMPC:cholesterol vesicles promote Aβ42 aggregation, we have provided a possible explanation for the proposed link between the disruption of cholesterol homeostasis and Alzheimer's disease. These results have been obtained by applying a chemical kinetics approach that allow us to dissect the overall macroscopic aggregation process of Aβ42 into its underlying component microscopic reactions. This strategy has led to the determination of the manner in which DMPC:cholesterol vesicles contribute to the early steps in Aβ42 aggregation by providing an alternative route for primary nucleation. The present work thus provides a clear example of the importance of understanding, in detail, the molecular mechanisms in which physiological factors can trigger the aggregation of Aβ42 in the complex molecular environment of the brain. As we have shown, these factors can dramatically reduce the typical timescale of Aβ42 aggregation, and thus their identification is crucial to understand the best points of intervention for strategies aimed at inhibiting or directing this process.

Methods

Theoretical analysis. *Kinetic analysis in the absence of lipids.* The aggregation of Aβ42 involves a process whereby secondary nucleation is responsible for the generation of most of the aggregates[31]. The aggregate mass concentration $M(t)$ and aggregate number concentration $P(t)$ can be described by the following differential equations[33]:

$$\frac{dP(t)}{dt} = k_n m(t)^{n_c} + k_2 m(t)^{n_2} M(t) \quad (1)$$

$$\frac{dM(t)}{dt} = 2m(t) k_+ P(t) \quad (2)$$

where the initial concentration of soluble monomers is denoted by $m(0)$, n_c and n_2 describe the dependencies of the primary and secondary nucleations on the monomer concentration, and k_n, k_+ and k_2 are the rate constants of primary nucleation, elongation and surface-catalysed secondary nucleation, respectively.

Using self-consistent methods, approximate analytical solutions to these differential equations can be obtained that describe the time evolution of the total fibril mass concentration, $M(t)$, as[31,32]:

$$\frac{M(t)}{M(\infty)} = 1 - \left(\frac{B_+ + C_+}{B_+ + C_+ e^{\kappa t}} \frac{B_- + C_+ e^{\kappa t}}{B_- + C_+} \right)^{\frac{k_\infty^2}{\kappa \widetilde{k}_\infty}} e^{-k_\infty t} \quad (3)$$

where $M(\infty) = m(0)$ is the final mass concentration of aggregates and:

$$B_\pm = \frac{k_\infty \pm \widetilde{k}_\infty}{2\kappa},\ C_\pm = \pm \frac{\lambda^2}{2\kappa^2},\ k_\infty = \sqrt{\frac{2\kappa^2}{n_2(n_2+1)} + \frac{2\lambda^2}{n_c}},\ \widetilde{k}_\infty = \sqrt{k_\infty^2 - 4C_+ C_- \kappa^2}$$

with $\lambda = \sqrt{2k_+ k_n m(0)^{n_c}}$ and $\kappa = \sqrt{2k_+ k_2 m(0)^{n_2+1}}$.

Note that, according to equation (3), to capture the complete macroscopic assembly process, only two particular combinations of the microscopic rate constants are needed, namely $k_+ k_n$ and $k_+ k_2$. These two combinations define the intrinsic timescales associated with the proliferation of new aggregates through primary pathways $\lambda = \sqrt{2k_+ k_n m(0)^{n_c}}$, and through secondary pathways $\kappa = \sqrt{2k_+ k_2 m(0)^{n_2+1}}$, respectively.

The experimental curves shown in Fig. 4c,d and Supplementary Fig. 12 were fitted using equation (3) where we introduced perturbations to λ and κ in order to account for the inclusion of the lipid–surface catalysed process. This procedure was carried out by adding to the rate constants of each of the microscopic steps a new factor, x, which allows the description of the experimental curves in the presence of the lipids, that is, $k' = k + x$. It was found that the best fits were derived when the rate of the primary pathways ($k_+ k_n$) was significantly increased and the rate of secondary pathways ($k_+ k_2$) was relatively unaffected. Coupled with other experiments (Fig. 4a-c) that support these fits, we observe that the lipid-catalysed process is mainly captured in the primary pathway, λ.

Theoretical model for a lipid-catalysed heterogeneous primary nucleation. The presence of low concentrations of DMPC:cholesterol vesicles introduces a new active process into the aggregation pathway of Aβ42, known as heterogeneous primary nucleation with the k_{cat} rate constant:

$$\frac{dP(t)}{dt} = k_n m(t)^{n_c} + k_{cat} m(t)^{n_h} s + k_2 m(t)^{n_2} M(t) \quad (4)$$

$$s = \sigma\{[L]/[P]\} \quad (5)$$

where s denotes the number of accessible sites for each peptide, which is a function of the lipid-to-protein ratio, [L]/[P]. σ is the surface accessibility constant, and n_h denotes the monomer concentration dependency of the heterogeneous nucleation pathway. It should be noted that the surface accessibility factor σ is dependent on the lipid system. In this particular study, σ is found to depend on the fraction of cholesterol in the DMPC:cholesterol membrane (Fig. 2b,c); in particular, σ is much greater with DMPC:cholesterol vesicles than with cholesterol-free ones. We rationalize the heterogeneous nucleation mechanism through the assumptions of the Langmuir adsorption isotherm, which indicates that the available lipid vesicles provide a surface for adsorption of Aβ42. This may facilitate nucleation and lead to the formation of Aβ42 primary oligomers on the surface of the vesicles.

Generalizing the self-consistent methods to the new kinetic equations, it is possible to obtain an approximate analytical solution for $M(t)$ in the presence of the additional nucleation mechanism (equation (4)) as:

$$\frac{M(t)}{M(\infty)} = 1 - \left(\frac{B_+' + C_+'}{B_+' + C_+' e^{\kappa' t}} \frac{B_-' + C_+' e^{\kappa' t}}{B_-' + C_+'} \right)^{\frac{k_\infty'^2}{\kappa' \widetilde{k}_\infty'}} e^{-k_\infty' t} \quad (6)$$

where $M(\infty)=m(0)$ as before and:

$$B'_{\pm}=\frac{k'_{\infty}\pm\widetilde{k'_{\infty}}}{2\kappa'},\ C'_{\pm}=\pm\frac{\lambda'^2}{2\kappa'^2},$$
$$k'_{\infty}=\sqrt{\frac{2\kappa'^2}{n_2(n_2+1)}+\frac{2\lambda'^2}{n_c}},\ \widetilde{k'_{\infty}}=\sqrt{k'^2_{\infty}-4C'_{+}C'_{-}\kappa'^2}$$

with $\kappa'=\kappa=\sqrt{2k_{+}k_2m(0)^{n_2+1}}$ and with a slight modification to λ, the primary pathway:

$$\lambda'=\sqrt{2k_{+}k_{n}m(0)^{n_c}+2k_{+}k_{cat}m(0)^{n_h}s} \quad (7)$$

Hence, the additional heterogeneous nucleation mechanism can be accounted for by a modification of the rate constant of primary nucleation, k_n, to give an effective rate constant k_n' that includes the heterogeneous nucleation pathway:

$$k'_{n}=k_{n}+k_{cat}m(0)^{n_h-n_c}s \quad (8)$$

In other words, the analytical solution in equation (6) is equivalent to equation (3) with a slight modification to λ that accounts for the presence of the additional primary pathway. Hence, kinetic traces of aggregation in the presence of heterogeneous primary nucleation can be analysed simply by using equation (3) (the analytical solution in the absence of lipids), but the extracted combined parameter for the primary pathway, k_+k_n', must be interpreted, using equation (8), as an effective parameter that includes the effect from the heterogeneous primary nucleation step.

Assuming that the homogeneous primary nucleation rate is unaffected by the introduction of the heterogeneous nucleation step, using equation (8), we can compute the (relative) acceleration $\varepsilon=\frac{k'_n}{k_n}$ of primary nucleation due to the presence of a heterogeneous primary step as:

$$\varepsilon=\frac{k'_{n}}{k_{n}}=1+\frac{\sigma k_{cat}m(0)^{(n_h-n_c)}[\mathrm{L}]\ /[\mathrm{P}]}{k_{n}} \quad (9)$$

and it is therefore dependent on the concentration of Aβ42. For a given lipid system where the accessibility factor σ is constant for various protein concentrations, the slope α of a plot of $\frac{k'_n}{k_n}$ versus [L]/[P]:

$$\alpha=\frac{k_{cat}m(0)^{(n_h-n_c)}}{k_{n}} \quad (10)$$

can be used to determine the reaction order for the heterogeneous primary nucleation step, n_h. Specifically, the slope of a double logarithmic plot of $\alpha m(0)^{n_c}$ against $m(0)$ is n_h (Fig. 4a). The low reaction order observed for n_h suggests that over the range of monomer concentrations probed in our experiments (1.5–3 μM), the coverage of monomers along a single primary nucleation site could be saturated. Specifically, we can model the rate of heterogeneous primary nucleation using a Langmuir adsorption isotherm model by replacing $m(0)$ by the monomer surface coverage $m(0)_{cov}=\frac{m(0)}{K+m(0)}$, where K is the equilibrium binding constant. When the coverage of the primary nucleation sites by the monomers is large ($m(0)>>K$), the Langmuir adsorption process is saturated, meaning that $m(0)_{cov}$ is independent of $m(0)$; hence, the saturation of primary nucleation sites could explain the observed low reaction order n_h of the heterogeneous primary nucleation step with respect to the monomer concentration.

In the presence of a large number of accessible primary nucleation sites, the rate of heterogeneous primary nucleation is constrained by the availability of free Aβ42 monomers that could adsorb onto a primary nucleation site at any point of time, rather than by the lipid concentration, so the rate laws become:

$$k'_{n}=k_{n}+k_{cat}\mathrm{max} \quad (11)$$

where $k_{cat}max=k_{cat}s_{max}$, and:

$$\frac{k_{+}k'_{n}}{k_{+}k_{n}}=1+\frac{k_{cat}\mathrm{max}}{k_{n}} \quad (12)$$

By taking the maximum increase of k_+k_n'/k_+k_n into account (Fig. 4f), we can conclude that the contribution of the heterogeneous primary nucleation increases the overall rate of primary nucleation by maximum 20-fold (equation (7)).

From the approximate analytical solution equation (3), $t_{1/2}$ is found to occur at[64–66]:

$$t_{1/2}\approx\log\left(\frac{1}{C_{+}}\right)\kappa^{-1} \quad (13)$$

Thus, if we consider solely an increase in the rate of primary nucleation, k_n' by 20 times, λ, the primary nucleation pathway, would increase by approximately $\sqrt{20}$ times. Correspondingly, $C_+=\frac{\lambda^2}{2\kappa^2}$ would increase by approximately 20 times, with no change in κ (equation (3)). Hence, the relative increase in $t_{1/2}$ due to the additional heterogeneous primary nucleation step is estimated to be 1/log(20) relative to the rate of the homogeneous primary nucleation, which is ≈34%.

Estimate in the number of primary nucleation sites. Under the assumption of the process of random and independent packing of cholesterol molecules on the surface of lipid vesicles, the probability of finding m-tuples of occupied adjacent primary nucleation sites is:

$$p=\theta^{m} \quad (14)$$

where θ is the surface coverage by cholesterol, that is, the fraction of primary nucleation sites covered by cholesterol molecules (the percentage of cholesterol within the membrane). Because $s=\sigma\{[L]/[P]\}$ (equation (5)), $\sigma\sim\theta^m$.

As we defined earlier (equation (10)), the slope α of a plot of $\frac{k'_n}{k_n}$ versus lipid concentration [L] depends on both σ and the concentration of monomer. Thus, for a constant protein concentration but different lipid systems (DMPC with different proportions of cholesterol), α can be used to determine σ. Because $\sigma\sim\theta^m$, the slope of a double logarithmic plot of α against the percentage of cholesterol within the membrane, θ, we find that $m\approx3$ according to Fig. 5b.

At given monomer and lipid concentrations, we can thus estimate the number of accessible primary nucleation sites per Aβ42 monomer:

$$r_{sites}=\{P(s)[\mathrm{lipid}]\}\ /\ m(0) \quad (15)$$

By taking the [L]/[P] ratio at which maximal acceleration of 2 μM Aβ42 aggregation is observed for the different cholesterol concentrations, the average r_{sites} is found to be between 0.05 and 0.20 (Table 1).

Data availability . The data that support the findings of this study are available from the authors upon reasonable request.

Received: 23 January 2017; Accepted: 20 February 2018;
Published online: 7 May 2018

References

1. Alzheimer's Association. 2012 Alzheimer's disease facts and figures. *Alzheimer's Dement* **8**, 131–168 (2012).
2. Dobson, C. M. Protein folding and misfolding. *Nature* **426**, 884–890 (2003).
3. Haass, C. & Selkoe, D. J. Soluble protein oligomers in neurodegeneration: lessons from the Alzheimer's amyloid beta-peptide. *Nat. Rev. Mol. Cell Biol.* **8**, 101–112 (2007).
4. Knowles, T. P. J., Vendruscolo, M. & Dobson, C. M. The amyloid state and its association with protein misfolding diseases. *Nat. Rev. Mol. Cell Biol.* **15**, 384–396 (2014).
5. Tanzi, R. E. & Bertram, L. Twenty years of the Alzheimer's disease amyloid hypothesis: a genetic perspective. *Cell* **120**, 545–555 (2005).
6. Necula, M., Kayed, R., Milton, S. & Glabe, C. G. Small molecule inhibitors of aggregation indicate that amyloid β oligomerization and fibrillization pathways are independent and distinct. *J. Biol. Chem.* **282**, 10311–10324 (2007).
7. Lansbury, P. T. & Lashuel, H. A. A century-old debate on protein aggregation and neurodegeneration enters the clinic. *Nature* **443**, 774–779 (2006).
8. Galvagnion, C. et al. Lipid vesicles trigger α-synuclein aggregation by stimulating primary nucleation. *Nat. Chem. Biol.* **11**, 229–234 (2015).
9. Di Paolo, G. & Kim, T.-W. Linking lipids to Alzheimer's disease: cholesterol and beyond. *Nat. Rev. Neurosci.* **12**, 284–296 (2011).
10. Gellermann, G. P. et al. Raft lipids as common components of human extracellular amyloid fibrils. *Proc. Natl Acad. Sci. USA* **102**, 6297–6302 (2005).
11. Bertram, L. & Tanzi, R. E. Thirty years of Alzheimer's disease genetics: the implications of systematic meta-analyses. *Nat. Rev. Neurosci.* **9**, 768–778 (2008).
12. Corder, E. H. et al. Gene dose of apolipoprotein E type 4 allele and the risk of Alzheimer's disease in late onset families. *Science* **261**, 921–923 (1993).
13. Bu, G. Apolipoprotein E and its receptors in Alzheimer's disease: pathways, pathogenesis and therapy. *Nat. Rev. Neurosci.* **10**, 333–344 (2009).
14. Holtzman, D. M. Role of apoE/Aβ interactions in the pathogenesis of Alzheimer's disease and cerebral amyloid angiopathy. *J. Mol. Neurosci.* **17**, 147–155 (2001).
15. Popp, J. et al. Cerebral and extracerebral cholesterol metabolism and CSF markers of Alzheimer's disease. *Biochem. Pharmacol.* **86**, 37–42 (2013).
16. Mori, T. et al. Cholesterol accumulates in senile plaques of Alzheimer disease patients and in transgenic APP(SW) mice. *J. Neuropathol. Exp. Neurol.* **60**, 778–785 (2001).

17. Zissimopoulos, J. M. et al. Sex and race differences in the association between statin use and the incidence of Alzheimer disease. *JAMA Neurol.* **111**, 390–400 (2016).
18. Dietschy, J. M. & Turley, S. D. Cholesterol metabolism in the brain. *Curr. Opin. Lipidol.* **12**, 105–112 (2001).
19. Vance, J. E. Dysregulation of cholesterol balance in the brain: contribution to neurodegenerative diseases. *Dis. Model. Mech.* **5**, 746–755 (2012).
20. Wood, W. G., Li, L., Müller, W. E. & Eckert, G. P. Cholesterol as a causative agent in Alzheimer disease a debatable hypothesis. *J. Neurochem.* **129**, 559–572 (2014).
21. Di Scala, C., Chahinian, H., Yahi, N., Garmy, N. & Fantini, J. Interaction of Alzheimer's β-amyloid peptides with cholesterol: mechanistic insights into amyloid pore formation. *Biochemistry* **53**, 4489–4502 (2014).
22. Michaels, T. C. T., Lazell, H. W., Arosio, P. & Knowles, T. P. J. Dynamics of protein aggregation and oligomer formation governed by secondary nucleation. *J. Chem. Phys.* **143**, 54901 (2015).
23. Arosio, P., Vendruscolo, M., Dobson, C. M. & Knowles, T. P. J. Chemical kinetics for drug discovery to combat protein aggregation diseases. *Trends Pharmacol. Sci.* **35**, 127–135 (2014).
24. Ghribi, O., Larsen, B., Schrag, M. & Herman, M. M. High cholesterol content in neurons increases BACE, β-amyloid, and phosphorylated tau levels in rabbit hippocampus. *Exp. Neurol.* **200**, 460–467 (2006).
25. Barrett, P. J. et al. The amyloid precursor protein has a flexible transmembrane domain and binds cholesterol. *Science* **117**, 2010–2013 (2012).
26. Evangelisti, E. et al. Membrane lipid composition and its physicochemical properties define cell vulnerability to aberrant protein oligomers. *J. Cell Sci.* **125**, 2416–2427 (2012).
27. Hellstrand, E., Sparr, E. & Linse, S. Retardation of Aβ fibril formation by phospholipid vesicles depends on membrane phase behavior. *Biophys. J.* **98**, 2206–2214 (2010).
28. Yip, C. M., Elton, E. A Darabie, A. A., Morrison, M. R. & McLaurin, J. Cholesterol, a modulator of membrane-associated A beta-fibrillogenesis and neurotoxicity. *J. Mol. Biol.* **311,** 723–734 (2001).
29. Hellstrand, E., Boland, B., Walsh, D. M. & Linse, S. Amyloid β-protein aggregation produces highly reproducible kinetic data and occurs by a two-phase process. *ACS Chem. Neurosci.* **1**, 13–18 (2010).
30. Knowles, T. P. J. et al. An analytical solution to the kinetics of breakable filament assembly. *Science* **326**, 1533–1537 (2009).
31. Cohen, S. I. A. et al. Proliferation of amyloid-β42 aggregates occurs through a secondary nucleation mechanism. *Proc. Natl Acad. Sci. USA* **110**, 9758–9763 (2013).
32. Cohen, S. I. A., Vendruscolo, M., Dobson, C. M. & Knowles, T. P. J. From macroscopic measurements to microscopic mechanisms of protein aggregation. *J. Mol. Biol.* **421**, 160–171 (2012).
33. Meisl, G. et al. Molecular mechanisms of protein aggregation from global fitting of kinetic models. *Nat. Protoc.* **11**, 252–272 (2016).
34. Meisl, G., Yang, X., Frohm, B., Knowles, T. P. J. & Linse, S. Quantitative analysis of intrinsic and extrinsic factors in the aggregation mechanism of Alzheimer-associated Aβ-peptide. *Sci. Rep.* **6**, 18728 (2016).
35. Meisl, G. et al. Differences in nucleation behavior underlie the contrasting aggregation kinetics of the Aβ40 and Aβ42 peptides. *Proc. Natl Acad. Sci. USA* **111**, 9384–9389 (2014).
36. Arosio, P. et al. Kinetic analysis reveals the diversity of microscopic mechanisms through which molecular chaperones suppress amyloid formation. *Nat. Commun.* **7**, 10948 (2016).
37. Cohen, S. I. A. et al. A molecular chaperone breaks the catalytic cycle that generates toxic Aβ oligomers. *Nat. Struct. Mol. Biol.* **22**, 207–213 (2015).
38. Sormanni, P., Aprile, F. A. & Vendruscolo, M. Rational design of antibodies targeting specific epitopes within intrinsically disordered proteins. *Proc. Natl Acad. Sci. USA* **112**, 9902–9907 (2015).
39. Habchi, J. et al. An anti-cancer drug suppresses the primary nucleation reaction that initiates the formation of toxic Aβ aggregates associated with Alzheimer's disease. *Sci. Adv.* **2**, e1501244 (2016).
40. Habchi, J. et al. Systematic development of small molecules to inhibit specific microscopic steps of Aβ42 aggregation in Alzheimer's disease. *Proc. Natl Acad. Sci. USA* **114**, E200–E208 (2016).
41. Sastry, P. S. Lipids of nervous tissue: composition and metabolism. *Prog. Lipid Res.* **24**, 69–176 (1985).
42. van Meer, G., Voelker, D. R. & Feigenson, G. W. Membrane lipids: where they are and how they behave. *Nat. Rev. Mol. Cell Biol.* **9**, 112–124 (2008).
43. Mouritsen, O. G. *Life—As a Matter of Fat* (Springer, Berlin, 2005).
44. Cotman, C. W., Blank, M., Moehl, A. & Snyder, F. Lipid composition of synaptic plasma membranes isolated from rat brain by zonal centrifugation. *Biochemistry* **8**, 4606–4612 (1969).
45. Nagle, J. F. et al. X-ray structure determination of fully hydrated L alpha phase dipalmitoylphosphatidylcholine bilayers. *Biophys. J.* **70**, 1419–1431 (1996).
46. Kucerka, N. et al. Structure of fully hydrated fluid phase DMPC and DLPC lipid bilayers using X-ray scattering from oriented multilamellar arrays and from unilamellar vesicles. *Biophys. J.* **88**, 2626–2637 (2005).
47. Chi, E. Y. et al. Lipid membrane templates the ordering and induces the fibrillogenesis of Alzheimer's disease amyloid-β peptide. *Prot. Struct. Funct. Genet.* **72**, 1–24 (2008).
48. Niu, Z. et al. The molecular structure of Alzheimer β-amyloid fibrils formed in the presence of phospholipid vesicles. *Angew. Chem. Int. Ed.* **53**, 9294–9297 (2014).
49. Simons, K. & Vaz, W. L. C. Model systems, lipid rafts, and cell membranes. *Annu. Rev. Biophys. Biomol. Struct.* **33**, 269–295 (2004).
50. Filippov, A., Orädd, G. & Lindblom, G. The effect of cholesterol on the lateral diffusion of phospholipids in oriented bilayers. *Biophys. J.* **84**, 3079–3086 (2003).
51. Barrett, M. A. et al. Solubility of cholesterol in lipid membranes and the formation of immiscible cholesterol plaques at high cholesterol concentrations. *Soft Matter* **9**, 9342–9351 (2013).
52. Almeida, P. F., Vaz, W. L. & Thompson, T. E. Lateral diffusion in the liquid phases of dimyristoylphosphatidylcholine/cholesterol lipid bilayers: a free volume analysis. *Biochemistry* **31**, 6739–6747 (1992).
53. Blume, A. A comparative study of the phase transitions of phospholipid bilayers and monolayers. *Biochim. Biophys. Acta Biomembr.* **557**, 32–44 (1979).
54. Wimley, W. C. & Thompson, T. E. Transbilayer and interbilayer phospholipid exchange in dimyristoylphosphatidylcholine/dimyristoylphosphatidylethanolamine large unilamellar vesicles. *Biochemistry* **30**, 1702–1709 (1991).
55. Harris, F. M., Best, K. B. & Bell, J. D. Use of laurdan fluorescence intensity and polarization to distinguish between changes in membrane fluidity and phospholipid order. *Biochim. Biophys. Acta Biomembr.* **1565**, 123–128 (2002).
56. Aguilar, L. F. et al. Differential dynamic and structural behavior of lipid-cholesterol domains in model membranes. *PLoS One* **7**, e40254 (2012).
57. Galvagnion, C. et al. Chemical properties of lipids strongly affect the kinetics of the membrane-induced aggregation of α-synuclein. *Proc. Natl Acad. Sci. USA* **113**, 7065–7070 (2016).
58. De Meyer, F. & Smit, B. Effect of cholesterol on the structure of a phospholipid bilayer. *Proc. Natl Acad. Sci. USA* **106**, 3654–3658 (2009).
59. de Jongh, H. H. J., Goormaghtigh, E. & Killian, J. A. Analysis of circular dichroism spectra of oriented protein–lipid complexes: toward a general application. *Biochemistry* **33**, 14521–14528 (1994).
60. Linse, S. & Lund, M. Surface effects on aggregation kinetics of amyloidogenic peptides. *J. Am. Chem. Soc.* **136**, 11555–11850 (2014).
61. Ruggeri, F. S. et al. Nanoscale studies link amyloid maturity with polyglutamine diseases onset. *Sci. Rep.* **6**, 31155 (2016).
62. Zandomeneghi, G., Krebs, M. R. H., McCammon, M. G. & Fändrich, M. FTIR reveals structural differences between native beta-sheet proteins and amyloid fibrils. *Protein Sci.* **13**, 3314–3321 (2004).
63. Arosio, P., Knowles, T. P. J. & Linse, S. On the lag phase in amyloid fibril formation. *Phys. Chem. Chem. Phys.* **17**, 7606–7618 (2015).
64. Cohen, S. I. A., Vendruscolo, M., Dobson, C. M. & Knowles, T. P. J. Nucleated polymerization with secondary pathways. II. Determination of self-consistent solutions to growth processes described by non-linear master equations. *J. Chem. Phys.* **135**, 65106 (2011).
65. Cohen, S. I. A., Vendruscolo, M., Dobson, C. M. & Knowles, T. P. J. Nucleated polymerization with secondary pathways. III. Equilibrium behavior and oligomer populations. *J. Chem. Phys.* **135**, 65107 (2011).
66. Cohen, S. I. A. et al. Nucleated polymerization with secondary pathways. I. Time evolution of the principal moments. *J. Chem. Phys.* **135**, 65105 (2011).
67. Simons, M. et al. Cholesterol depletion inhibits the generation of β-amyloid in hippocampal neurons. *Proc. Natl Acad. Sci. USA* **95**, 6460–6464 (1998).
68. Hong, S. et al. Soluble Aβ oligomers are rapidly sequestered from brain ISF in vivo and bind GM1 ganglioside on cellular membranes. *Neuron* **82**, 308–319 (2014).

Acknowledgements

The authors acknowledge support from the Centre for Misfolding Diseases (J.H., S.C., T.C.T.M., M.M.J.B., F.S.R., M.S., J.R.K., C.M.D., T.P.J.K. and M.V.); the Agency for Science, Technology and Research, Singapore (S.C.); a Marie Skłodowska-Curie Actions — Individual Fellowship (C.G.); Peterhouse College, Cambridge (T.C.T.M.); the Swiss National Science Foundation (T.C.T.M., F.S.R.); the NIH-Oxford/Cambridge Scholars Program (M.M.J.B.); the Cambridge Commonwealth, European and International Trust (M.M.J.B.); the Knut & Alice Wallenberg Foundation (S.L., E.S.); the European Research Council (S.L.); the Swedish Research Council (S.L., E.S.) the Frances and Augustus Newman Foundation (T.P.J.K.); the UK Biotechnology and Biochemical Sciences Research Council (C.M.D. and M.V.); and the Wellcome Trust (C.M.D., T.P.J.K. and M.V.). This work was supported by the Intramural Research Program of the National Institute of Diabetes and Kidney Diseases, NIH.

Author contributions

J.H., S.C., C.G., T.C.T.M., E.S., S.L., C.M.D., T.P.J.K. and M.V. designed the research. J.H., S.C., C.G., F.S.R., M.S. and I.I. performed the research. J.H., S.C., C.G., F.S.R., I.I., J.R.K., E.S., S.L., C.M.D., T.P.J.K. and M.V. contributed reagents/analytic tools. J.H., S.C., C.G., T.C.T.M., M.M.J.B., F.S.R., E.S., S.L., C.M.D., T.P.J.K. and M.V. analysed the data. All authors discussed the results and contributed to the writing of the paper.

Competing interests

The authors declare no competing interests.

Additional information

Supplementary information is available for this paper at https://doi.org/10.1038/s41557-018-0031-x.

Reprints and permissions information is available at www.nature.com/reprints.

Correspondence and requests for materials should be addressed to M.V.

Publisher's note: Springer Nature remains neutral with regard to jurisdictional claims in published maps and institutional affiliations.